ELSEVIER

Composite Structures 56 (2002) 201–210

COMPOSITE STRUCTURES

www.elsevier.com/locate/compstruct

Bending behavior of filament-wound fiber-reinforced sandwich pipes

M. Xia [a,*], H. Takayanagi [a], K. Kemmochi [b]

[a] *Smart Structure Research Center, National Institute of Advanced Industrial Science and Technology, AIST Tsukuba Central 2, Tsukuba 305-8568, Japan*

[b] *Faculty of Textile Science and Technology, Shinehu University, Ueda 386-8567, Japan*

Abstract

Based on the classical laminated-plate theory, an exact solution is presented for multi-layered filament-wound composite pipes under pure bending. Moreover, detailed stress–strain responses and deflection for filament-wound fiber-reinforced sandwich pipes are investigated using the present analytical method. Sandwich pipes are created using resin material for the core layer and filament-wound composite for the skin layers. It is observed that the axial stress at the inner surface can be larger than that at the outer surface when the pipe has the filament-wound outer layers with high anisotropic materials. The cross-sectional shape of the pipes is no longer a circle even when the pipe is subjected to pure bending load. © 2002 Published by Elsevier Science Ltd.

1. Introduction

Sandwich-type pipes have been used in various industries for many years because of their high performance in terms of combining high stiffness with light weight. A typical sandwich pipe consists of two skins made of metals or laminated composites and a core layer. The core layer is usually made of metallic or nonmetallic resin material with low stiffness. In recent years, plastic foams have been used for core in sandwich structures due to their reduced weight and good thermal insulation.

Filament-wound composite pipes have been the subjects of numerous experimental investigations, as demonstrated in the literature [1–7]. Numerical methods have also been presented and used for estimating mechanical properties of filament-wound composite pipes [8–12]. However, most of these studies on cylindrical fiber-reinforced composite pipes have focused on thin-walled cylindrical shells. We know that design methods based on a thin-walled multi-layered shell are usually unsuitable for the design of thick-walled composite shell structures. To date, relatively little work has been done with regard to thick-walled cylindrical behavior and fiber-reinforced composite sandwich pipes in particular. For thick-walled composite sandwich pipes, Xia et al. [13,14] developed analytical procedures to assess the stress–strain responses and deflection under internal pressure loading and lateral compression [15], respectively. The procedures are based on the theories of laminated-plate and cylindrical orthotropy elasticity. Lo and Conway [16] have solved the general formulation and discussed the influence of Poisson's ratios on internal stress of multi-layered cylindrical pipe under bending load. The mismatch of Poisson's ratios between the layers induces stresses in composite structures. Lekhnitskii [17] provided formulations for anisotropic single-layer pipe subjected to bending load.

In the present study, on the basis of the laminated-plate theory, an analytical solution for multi-layered filament-wound composite pipes under bending load is provided using Lekhnitskii's stress function approach. The material for each layer is considered to be homogeneous or cylindrically orthotropic. Furthermore, the procedure is applied to an example of fiber-reinforced sandwich cylindrical pipe in which the core is made of isotropic material and the skins of filament-wound material. Stress–strain responses and deflection for the composite pipe subjected to the bending load are investigated.

2. Analytical procedure

The sandwich pipe is created using nonreinforced material for the core layer and alternate-ply materials for the skin layers. Alternate-ply skin layers are those in which the principal material directions of the adjacent

* Corresponding author. Tel.: +81-298-61-3128; fax: +81-298-61-3126.

E-mail address: ming.xia@aist.go.jp (M. Xia).

0263-8223/02/$ - see front matter © 2002 Published by Elsevier Science Ltd.
PII: S0263-8223(01)00181-7

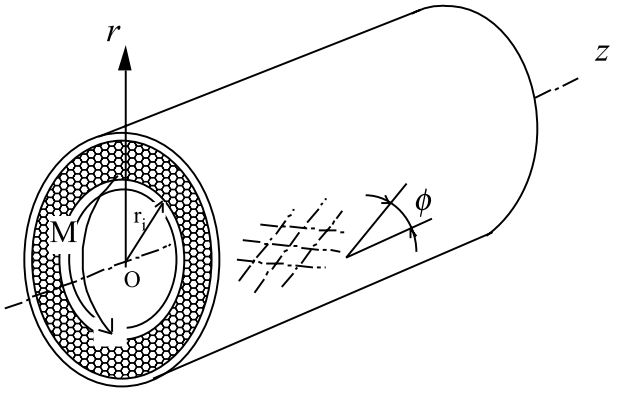

Fig. 1. Filament-wound sandwich pipe subjected to bending load.

layer have an opposite fiber orientation ($\pm\phi$) with respect to the axial direction. Fig. 1 shows the cylindrical coordinates for a sandwich composite pipe subjected to bending load.

2.1. Stress analysis

The two adjacent lay-ups are assumed to behave together as an orthotropic unit. According to the equations of the generalized Hooke's law, the stress–strain relations of each individual laminated pipe with cylindrical orthotropy are written as:

$$\begin{aligned}
\varepsilon_r &= S_{11}\sigma_r + S_{12}\sigma_\theta + S_{13}\sigma_z,\\
\varepsilon_\theta &= S_{12}\sigma_r + S_{22}\sigma_\theta + S_{23}\sigma_z,\\
\varepsilon_z &= S_{13}\sigma_r + S_{23}\sigma_\theta + S_{33}\sigma_z,\\
\gamma_{r\theta} &= S_{44}\tau_{r\theta},
\end{aligned} \tag{1}$$

where S_{ij} are the compliance constants with respect to the material symmetry. These constants in terms of engineering constants are obtained from Section 2.4.

The stress along the axial direction, σ_z, is given by [17]

$$\sigma_z = Ar\sin\theta - \frac{1}{S_{33}}(S_{13}\sigma_r + S_{23}\sigma_\theta). \tag{2}$$

Substituting Eq. (2) into the first and second expressions of Eq. (1), we obtain the constitutive equations:

$$\begin{aligned}
\varepsilon_r &= R_{11}\sigma_r + R_{12}\sigma_\theta + S_{13}Ar\sin\theta,\\
\varepsilon_\theta &= R_{12}\sigma_r + R_{22}\sigma_\theta + S_{23}Ar\sin\theta,
\end{aligned} \tag{3}$$

where the reduced compliance constants R_{ij} are expressed in terms of the compliance matrix S_{ij} as

$$R_{ij} = S_{ij} - \frac{S_{i3}S_{j3}}{S_{33}} \quad (i,j = 1,2,4). \tag{4}$$

By introducing a stress function $F(r,\theta)$, the stress fields can be expressed with the stress function as:

$$\begin{aligned}
\sigma_r &= \frac{1}{r}\frac{\partial F}{\partial r} + \frac{1}{r^2}\frac{\partial^2 F}{\partial\theta^2},\\
\sigma_\theta &= \frac{\partial^2 F}{\partial r^2},\\
\tau_{r\theta} &= -\frac{\partial^2}{\partial r\partial\theta}\left(\frac{F}{r}\right).
\end{aligned} \tag{5}$$

The stress function satisfies the following compatibility equation:

$$\frac{\partial^2\varepsilon_r}{\partial\theta^2} + r\frac{\partial^2(r\varepsilon_\theta)}{\partial r^2} - \frac{\partial^2(r\gamma_{r\theta})}{\partial r\partial\theta} - r\frac{\partial\varepsilon_r}{\partial r} = 0. \tag{6}$$

Substituting Eq. (3) into Eq. (6) and using Eq. (5), we obtain the following differential equation:

$$\begin{aligned}
&R_{22}\frac{\partial^4 F}{\partial r^4} + (2R_{12}+R_{44})\frac{1}{r^2}\frac{\partial^4 F}{\partial r^2\partial\theta^2} + R_{11}\frac{1}{r^4}\frac{\partial^4 F}{\partial\theta^4}\\
&\quad + 2R_{22}\frac{1}{r}\frac{\partial^3 F}{\partial r^3} - (2R_{12}+R_{44})\frac{1}{r^3}\frac{\partial^3 F}{\partial r\partial\theta^2} - R_{11}\frac{1}{r^2}\frac{\partial^2 F}{\partial r^2}\\
&\quad + (2R_{11}+2R_{12}+R_{44})\frac{1}{r^4}\frac{\partial^2 F}{\partial\theta^2} + R_{11}\frac{1}{r^3}\frac{\partial F}{\partial r}\\
&\qquad = 2(S_{13}-S_{23})A\frac{\sin\theta}{r}.
\end{aligned} \tag{7}$$

The stress function takes the form of the following Lekhnitskii's stress function:

$$F^{(k)}(r,\theta) = f(r)\sin\theta. \tag{8}$$

Substituting the stress function into Eq. (7), we obtain

$$\begin{aligned}
&R_{22}r^4 f^{(4)} + 2R_{22}r^3 f^{(3)} - (R_{11}+2R_{12}+R_{44})r^2 f''\\
&\quad + (R_{11}+2R_{12}+R_{44})rf' - (R_{11}+2R_{12}+R_{44})f\\
&\qquad = 2(S_{13}-S_{23})A\frac{\sin\theta}{r}.
\end{aligned} \tag{9}$$

The solution for Eq. (9) is given as

$$F(r,\theta) = \left(\frac{B}{\beta}r^{1+\beta} + \frac{C}{\beta}r^{1-\beta} + Dr\ln r + Er + \frac{A\eta}{2}r^3\right)\sin\theta, \tag{10}$$

where A, B, C, and D are the unknown constants of integration, and

$$\begin{aligned}
\beta &= \sqrt{1 + \frac{R_{11}+2R_{12}+R_{44}}{R_{22}}},\\
\eta &= \frac{S_{23}-S_{13}}{R_{11}+2R_{12}+R_{44}-3R_{22}}.
\end{aligned} \tag{11}$$

Considering that the displacements are single-valued functions of the coordinates, D can be set to zero.

According to Eqs. (5) and (9), the components of the stress fields can be expressed as

$$\begin{aligned}
\sigma_r &= (Br^{-1+\beta} - Cr^{-1-\beta} + A\eta r)\sin\theta,\\
\sigma_\theta &= [B(1+\beta)r^{-1+\beta} - C(1-\beta)r^{-1-\beta}\\
&\qquad + 3A\eta r]\sin\theta,\\
\tau_{r\theta} &= -(Br^{-1+\beta} - Cr^{-1-\beta} + A\eta r)\cos\theta.
\end{aligned} \tag{12}$$

Substituting Eq. (12) into (2), the stress along the axial direction is

$$\sigma_z = [s_1 B r^{-1+\beta} + s_2 C r^{-1-\beta} + s_3 A r]\sin\theta, \tag{13}$$

where

$$\begin{aligned} s_{1,2} &= \mp\frac{S_{13} + S_{23}(1\pm\beta)}{S_{33}}, \\ s_3 &= 1 - \frac{(S_{13}+3S_{23})\eta}{S_{33}}. \end{aligned} \tag{14}$$

2.2. Deflection analysis

The strain–displacement relations in the cylindrical coordinate can be described as:

$$\begin{aligned} \varepsilon_r^{(k)} &= \frac{\partial u_r^{(k)}}{\partial r}, \\ \varepsilon_\theta^{(k)} &= \frac{1}{r}\frac{\partial u_\theta^{(k)}}{\partial\theta} + \frac{u_r^{(k)}}{r}, \\ \gamma_{\theta r}^{(k)} &= \frac{1}{r}\frac{\partial u_r^{(k)}}{\partial\theta} + r\frac{\partial}{\partial r}\left(\frac{u_\theta^{(k)}}{r}\right). \end{aligned} \tag{15}$$

The solution of the first expression of Eq. (15) is obtained as

$$u_r = (p_1 B r^\beta + p_2 C r^{-\beta} + p_3 A r^2)\sin\theta + f(\theta), \tag{16}$$

where $f(\theta)$ is an unknown function of integration, and

$$\begin{aligned} p_{1,2} &= \frac{R_{11} + R_{12}(1\pm\beta)}{\beta}, \\ p_3 &= \frac{(R_{11}+3R_{12})\eta + S_{13}}{2}. \end{aligned} \tag{17}$$

Substituting Eq. (16) into the second expression of Eq. (15), we have the solution

$$u_\theta = \left(q_1 B r^\beta + q_2 C r^{-\beta} + q_3 A r^2\right)\cos\theta - \int f(\theta)\,\mathrm{d}\theta + g(r), \tag{18}$$

where $g(r)$ is an unknown function of integration, and

$$\begin{aligned} q_{1,2} &= \frac{R_{11} + R_{12} \mp R_{22}\beta(1\pm\beta)}{\beta}, \\ q_3 &= \frac{(R_{11}+R_{12}-6R_{22})\eta + S_{13} - 2S_{23}}{2}. \end{aligned} \tag{19}$$

Substituting Eqs. (16) and (18) into the third expression of Eq. (15), we obtain the following differential equation:

$$\frac{\partial f(\theta)}{\partial\theta} + \int f(\theta)\,\mathrm{d}\theta + r\frac{\partial g(r)}{\partial r} - g(r) = 0, \tag{20}$$

which has the following solution:

$$\begin{aligned} g(r) &= Fr, \\ f(\theta) &= H\sin\theta + J\cos\theta, \end{aligned} \tag{21}$$

where F, H and J are the unknown constants of integration.

The displacements obtained from Eqs. (16) and (18) are then:

$$\begin{aligned} u_r &= \left(p_1 B r^\beta + p_2 C r^{-\beta} + p_3 A r^2\right)\sin\theta \\ &\quad + H\sin\theta + J\cos\theta, \\ u_\theta &= \left(q_1 B r^\beta + q_2 C r^{-\beta} + q_3 A r^2\right)\cos\theta \\ &\quad + H\cos\theta - J\sin\theta + Fr. \end{aligned} \tag{22}$$

According to geometric symmetry

$$\begin{aligned} u_r(\theta) &= u_r(\pi-\theta), \\ u_\theta(\theta) &= -u_\theta(\pi-\theta). \end{aligned} \tag{23}$$

Therefore, we obtain $J = F = 0$.

Putting $u_r = u_\theta = 0$ in the initial condition that the applied moment $M = 0$, Eq. (22) leads to $H = 0$.

As shown in Fig. 2, the displacements in the x'–y' coordinate system can be expressed as:

$$\begin{aligned} \Delta x' &= u_r\cos\theta - u_\theta\sin\theta, \\ \Delta y' &= u_r\sin\theta + u_\theta\cos\theta. \end{aligned} \tag{24}$$

The deformation curves for the cross-section of the pipe subjected to bending load are given as:

$$\begin{aligned} x' &= r_i\cos\theta + \frac{u_r^0 - u_\theta^0}{2}\sin 2\theta, \\ y' &= r_i\sin\theta - \frac{u_r^0 + u_\theta^0}{2} + \frac{u_r^0 - u_\theta^0}{2}\cos 2\theta. \end{aligned} \tag{25}$$

2.3. Boundary conditions

Assuming that the interfaces between the core and skin layers are perfectly bound, the continuance of displacements, tractions along the interfaces and traction-

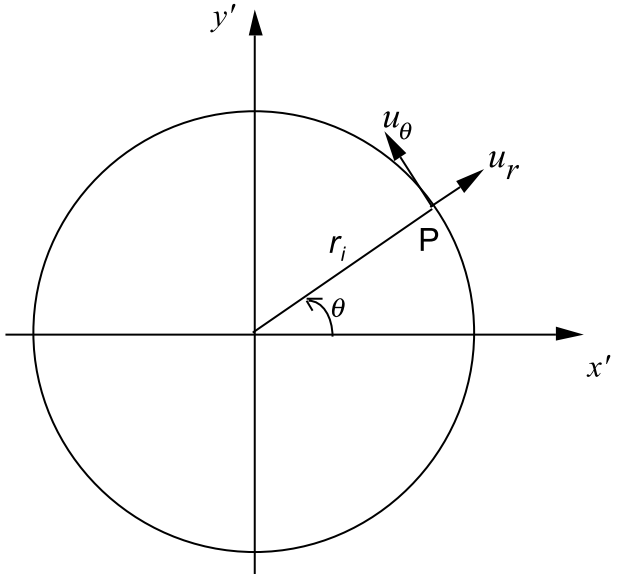

Fig. 2. Coordinate system through cross-sectional shape.

free boundary conditions provide a homogeneous equation.

The conditions on the cylindrical inner and outer surfaces are:

$$\begin{aligned}&\sigma_r(r_0)=\tau_{r\theta}(r_0)=0,\\&\sigma_r(r_a)=\tau_{r\theta}(r_a)=0.\end{aligned}\tag{26}$$

The continuity conditions for the displacements and stresses in the interfaces lead to:

$$\begin{aligned}&u_r^{(k)}(r_k)=u_r^{(k+1)}(r_k),\\&u_\theta^{(k)}(r_k)=u_\theta^{(k+1)}(r_k),\\&\tau_{r\theta}^{(k)}(r_k)=\tau_{r\theta}^{(k+1)}(r_k),\\&\sigma_r^{(k)}(r_k)=\sigma_r^{(k+1)}(r_k),\quad k=1,2,\ldots,n.\end{aligned}\tag{27}$$

The equilibrium for bending moment is satisfied by the following relation:

$$\int\int_S \sigma_z r^2\sin\theta\,\mathrm{d}r\,\mathrm{d}\theta=M.\tag{28}$$

Eqs. (26)–(28) can give a set of equations to determine unknown constants. For a pipe with N-layers, there exist $3N$ constants. Using $3(N-1)$ continuity conditions (27), the two free surface conditions (26), and an equilibrium condition of bending moment (28), the constants can be determined by the solution of a homogeneous equation. Notice that the radial stress σ_r and the shear stress $\tau_{r\theta}$ in Eqs. (26) and (27) are identical boundary conditions.

For the filament-winding pipe with single layer, the unknown constants can be given as:

$$\begin{aligned}A&=\frac{M}{K},\\B&=-\frac{\eta M}{K}\frac{r_a^{2+\beta}-r_0^{2+\beta}}{r_a^{2\beta}-r_0^{2\beta}},\\C&=\frac{\eta M}{K}\frac{r_a^{2-\beta}-r_0^{2-\beta}}{r_a^{-2\beta}-r_0^{-2\beta}},\end{aligned}\tag{29}$$

where

$$\begin{aligned}K=\frac{\pi}{4}(r_a^4-r_0^4)-\frac{\eta\pi}{S_{33}}\Bigg[&\frac{S_{13}+3S_{23}}{4}(r_a^4-r_0^4)\\&-\frac{S_{13}+S_{23}(1+\beta)}{2+\beta}\frac{\left(r_a^{2+\beta}-r_0^{2+\beta}\right)^2}{r_a^{2\beta}-r_0^{2\beta}}\\&-\frac{S_{13}+S_{23}(1-\beta)}{2-\beta}\frac{\left(r_a^{2-\beta}-r_0^{2-\beta}\right)^2}{r_a^{-2\beta}-r_0^{-2\beta}}\Bigg].\end{aligned}\tag{30}$$

For the core layer with the isotropic material, then $\eta=0$ and $\beta=2$.

For the isotropic pipe with a single layer, the distribution of stresses will be:

$$\begin{aligned}&\sigma_z=\frac{M}{I}r\sin\theta,\\&\sigma_r=\sigma_\theta=\tau_{r\theta}=0,\end{aligned}\tag{31}$$

where $I=(\pi/4)(r_a^4-r_0^4)$ is the moment of inertia of the cross-section.

2.4. Transformation from ply properties to laminate properties

The relationship of stresses and strains between the cylindrical and principal coordinate systems is given, respectively, by

$$\begin{aligned}&\begin{Bmatrix}\sigma_z\\\sigma_y\\\sigma_x\\\tau_{zy}\\\tau_{yx}\\\tau_{xz}\end{Bmatrix}=(P_{ij})\begin{Bmatrix}\sigma_r\\\sigma_\theta\\\sigma_z\\\tau_{r\theta}\\\tau_{\theta z}\\\tau_{zr}\end{Bmatrix}\quad\text{and}\\&\begin{Bmatrix}\varepsilon_z\\\varepsilon_y\\\varepsilon_x\\\gamma_{zy}\\\gamma_{yx}\\\gamma_{xz}\end{Bmatrix}=(Q_{ij})\begin{Bmatrix}\varepsilon_r\\\varepsilon_\theta\\\varepsilon_z\\\gamma_{r\theta}\\\gamma_{\theta z}\\\gamma_{zr}\end{Bmatrix},\end{aligned}\tag{32}$$

where (P_{ij}) and (Q_{ij}) are the coordinate transformation matrices between the on-axis and the cylindrical axis shown in Fig. 3

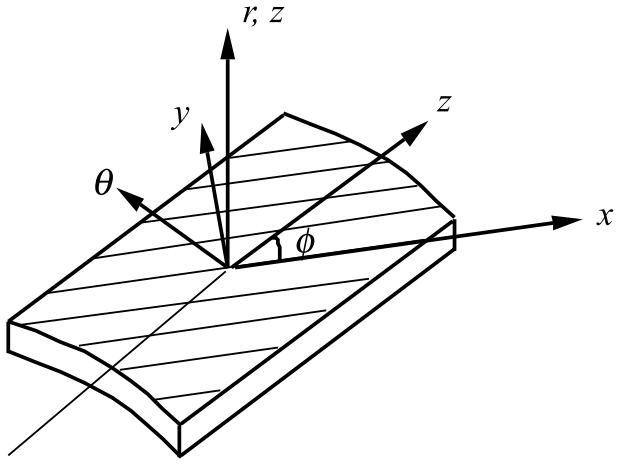

Fig. 3. Relation of coordinate system between principal material axis and cylindrical axes.

$$(P_{ij}) = \begin{Bmatrix} 1 & 0 & 0 & 0 & 0 & 0 \\ 0 & m^2 & n^2 & 0 & -2mn & 0 \\ 0 & n^2 & m^2 & 0 & 2mn & 0 \\ 0 & 0 & 0 & m & 0 & -n \\ 0 & mn & -mn & 0 & m^2-n^2 & 0 \\ 0 & 0 & 0 & n & 0 & m \end{Bmatrix},$$

$$(Q_{ij}) = \begin{Bmatrix} 1 & 0 & 0 & 0 & 0 & 0 \\ 0 & m^2 & n^2 & 0 & -mn & 0 \\ 0 & n^2 & m^2 & 0 & mn & 0 \\ 0 & 0 & 0 & m & 0 & -n \\ 0 & 2mn & -2mn & 0 & m^2-n^2 & 0 \\ 0 & 0 & 0 & n & 0 & m \end{Bmatrix} \tag{33}$$

and $m = \cos\phi,\ n = \sin\phi$.

Owing to the symmetric and material symmetry with the x and y axes, respectively, the stress–strain relation under the principal coordinate system is given as

$$\begin{Bmatrix} \varepsilon_z \\ \varepsilon_y \\ \varepsilon_x \\ \gamma_{zy} \\ \gamma_{yx} \\ \gamma_{xz} \end{Bmatrix} = \begin{bmatrix} a_{11} & a_{12} & a_{13} & 0 & 0 & 0 \\ a_{12} & a_{11} & a_{13} & 0 & 0 & 0 \\ a_{13} & a_{13} & a_{33} & 0 & 0 & 0 \\ 0 & 0 & 0 & 2(a_{11}-a_{12}) & 0 & 0 \\ 0 & 0 & 0 & 0 & a_{44} & 0 \\ 0 & 0 & 0 & 0 & 0 & a_{44} \end{bmatrix} \times \begin{Bmatrix} \sigma_z \\ \sigma_y \\ \sigma_x \\ \tau_{zx} \\ \tau_{yx} \\ \tau_{xz} \end{Bmatrix}, \tag{34}$$

where matrix (a_{ij}) can be obtained from engineering constants defined as

$$\begin{aligned} a_{11} &= 1/E_y, \\ a_{33} &= 1/E_x, \\ a_{44} &= 1/G_{zz}, \\ a_{12} &= -v_{zy}/E_y, \\ a_{13} &= -v_{yx}/E_x. \end{aligned} \tag{35}$$

According to Eqs. (32) and (34), the stress–strain relation under the cylindrical coordinate system is

$$\begin{Bmatrix} \varepsilon_r \\ \varepsilon_\theta \\ \varepsilon_z \\ \gamma_{r\theta} \\ \gamma_{\theta z} \\ \gamma_{zr} \end{Bmatrix} = (Q_{ij})^{-1}(a_{ij})(P_{ij}) \begin{Bmatrix} \sigma_r \\ \sigma_\theta \\ \sigma_z \\ \tau_{r\theta} \\ \tau_{\theta z} \\ \tau_{zr} \end{Bmatrix}. \tag{36}$$

Comparing Eq. (36) with Eq. (1), we can obtain the compliance constants from

$$(S_{ij}) = (Q_{ij})^{-1}(a_{ij})(P_{ij}). \tag{37}$$

3. Numerical results and discussion

The procedure is applied to an example of a composite sandwich pipe with an isotropic-core layer and orthotropic-skin layers. The elasticity solutions are obtained when a bending moment of 0.25 kN m is applied. The pipe has an inner radius of 50 mm, a core-layer thickness of 20 mm, and skin-layer thickness of 2 mm. In order to obtain the effects of cylindrical material anisotropy and fiber orientation on the response of the pipe under a bending moment, the stress and strain behaviors of a sandwich pipe are investigated based on carbon fiber/epoxy (T300/934) and E-glass/epoxy [18]. In the present study, the inner and outer pipes of the sandwich structure are made of the same material. The material properties used in this study are given in Table 1.

For any cross-section of cylindrical pipe, the stress and strain vary with the angle θ. The hoop and axial stresses at $\theta = \pm\pi/2$ show the maximum tensile or compressive stress while the pipes are subjected to maximum shear stresses at $\theta = 0$ and π. In the following analytical results, the stresses and strains are calculated along the positive y-direction for $\theta = \pi/2$ (see Fig. 2).

Figs. 4 and 5, respectively, show the axial and hoop stress curves varying with the winding angle under the bending load. The effect of the winding angle on stress variation is much larger for the carbon fiber (T300/934) than for the glass fiber (E-glass/epoxy) because the carbon fiber material has larger anisotropic properties. As shown in Fig. 4, both inner and outer surfaces of the sandwich pipe are subjected to almost constant axial stresses when the winding angle is larger than 60°, and the axial stress at the outer surface displays a larger value than that at the inner surface. For a pipe within a certain range of winding angles, however, it is observed that the axial stress at the inner surface displays a larger value than that at the outer. It is well known that this situation should be prevented in the case of pipes with isotropic or lower anisotropic materials. In Fig. 5, the hoop stress at the inner surface is greater than that at the outer surface. Both inner and outer surfaces are subjected to alternative stresses by varying the winding angle.

Figs. 6 and 7 show the comparison of the present elasticity theory with the general solution. The elastic

Table 1
Material properties of skin layers and resin

Properties	T300/934	E-glass/epoxy	Resin (core)
E_x (GPa)	141.6	43.4	1.2
E_y (GPa)	10.7	15.2	1.2
G_{zz} (GPa)	3.88	6.14	0.46
v_{yx}	0.268	0.29	0.30
v_{zy}	0.495	0.38	0.30

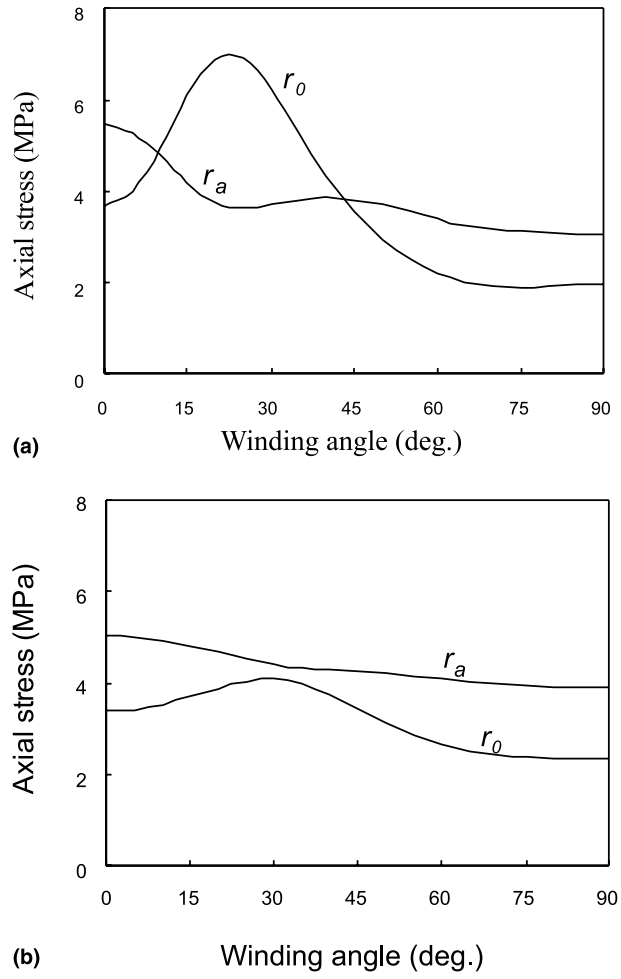

Fig. 4. Effect of the winding angle on the axial stresses of pipe with (a) T300/934 and (b) E-glass/epoxy.

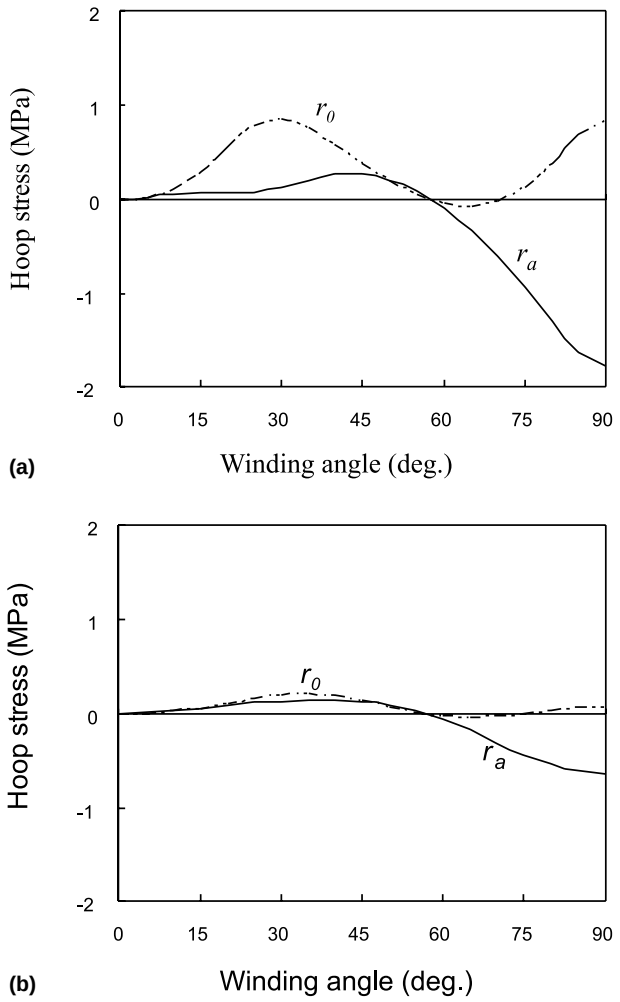

Fig. 5. Effect of the winding angle on the hoop stresses of pipe with (a) T300/934 and (b) E-glass/epoxy.

modulus (E_{axial}) in the axial direction with the winding angle is calculated by the following expression [19]:

$$1/E_{\text{axial}} = 1/\overline{E} - \psi^2 \overline{G}, \tag{38}$$

where

$$\begin{aligned}
\frac{1}{\overline{E}} &= \frac{\cos^4\phi}{E_{\text{L}}} + \left(\frac{1}{G_{zz}} - \frac{2\nu_{\text{L}}}{E_{\text{L}}}\right) \\
&\quad \times \sin^2\phi\cos^2\phi + \frac{\sin^4\phi}{E_{\text{T}}}, \\
\frac{1}{\overline{G}} &= \left(\frac{1+\nu_{\text{L}}}{E_{\text{L}}} + \frac{1+\nu_{\text{T}}}{E_{\text{T}}}\right)\sin^2 2\phi \\
&\quad + \frac{1}{G_{zz}}\cos^2 2\phi, \\
\psi &= \left[\frac{\sin^2\phi}{E_{\text{T}}} - \frac{\cos^2\phi}{E_{\text{L}}} \right. \\
&\quad \left. + \frac{1}{2}\left(\frac{1}{G_{zz}} - \frac{2\nu_{\text{L}}}{E_{\text{L}}}\right)\cos 2\phi\right]\sin 2\phi
\end{aligned} \tag{39}$$

and ϕ is the winding angle.

According to the general analytical method without considering the hoop and the radial stresses, the axial stress under the bending load is given as

$$\sigma_z = \frac{E_{\text{axial}} r_i}{\overline{EI}} M, \tag{40}$$

where

$$\begin{aligned}
\overline{EI} &= \frac{\pi R_0^4 E_{\text{axial}}}{4}\left\{[(1+t_f/R_0)^4 - 1\right. \\
&\quad + (R/R_0)^4 - (R/R_0 - t_f/R_0)^4] \\
&\quad + \left(\frac{E_{\text{core}}}{E_{\text{axial}}}\right)[(R/R_0 - t_f/R_0)^4 \\
&\quad \left. - (1+t_f/R_0)^4]\right\}.
\end{aligned} \tag{41}$$

As shown in Figs. 6 and 7, the axial stresses have the same values for two analytical methods when pipes are wound at 0°. This is because the pipe with 0°-winding angle is the transverse isotropy. A significant difference

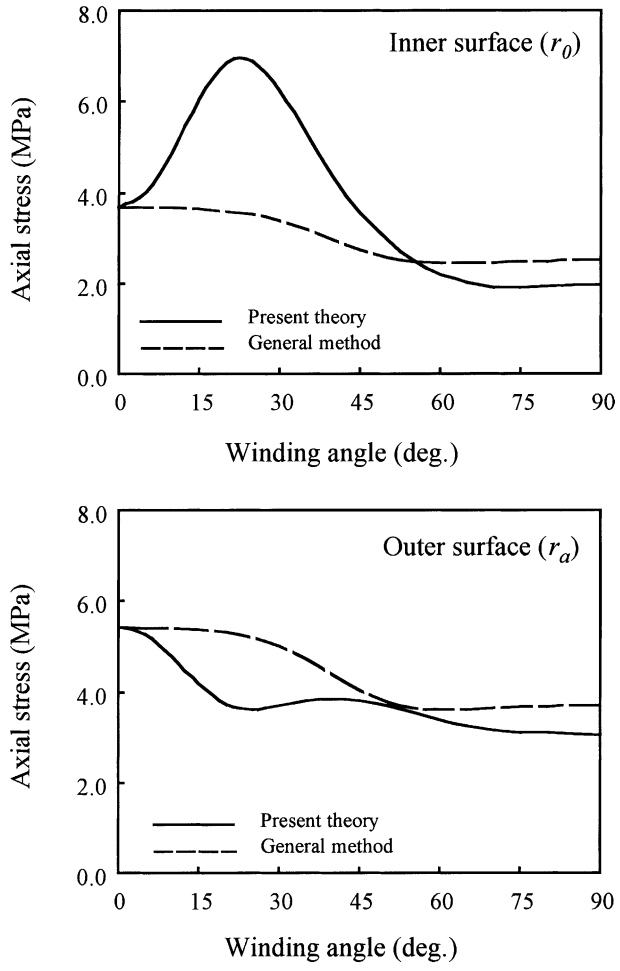

Fig. 6. Comparison of the present theory with the general method (T300/934).

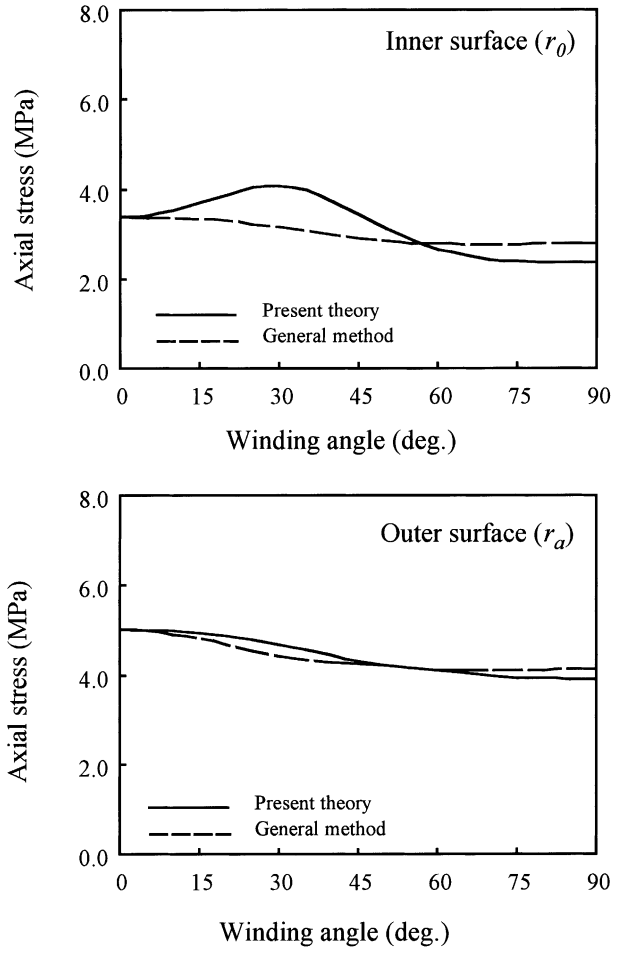

Fig. 7. Comparison of the present theory with the general method (E-glass/epoxy).

is revealed between the present theory and the general solution when the pipes have high anisotropy. For the isotropic materials, the results obtained from the present elasticity theory coincide with those from the general method.

The radial stresses at the surfaces of the pipe are equal to zero due to the free traction at the inner and outer surfaces. For the two interfaces between the core and skins, the variation of the radial stress with the winding angle is shown in Fig. 8. The radial stresses at the interfaces may be tensile or compressive for pipes with different winding angles. The outer interface is subjected to larger radial stress than the inner interface when the winding angle varies from zero to about 58°, while the inner interface has higher stress when the winding angle is larger than 58°. For a pipe with longitudinal fiber orientation ($\phi = 0$), it is observed from Figs. 5 and 8 that the hoop and radial stresses equal zero. This is because stress states degenerate into those of isotropic materials in the case of the transverse isotropy ($\eta = 0$) of composites with respect to the longitudinal direction.

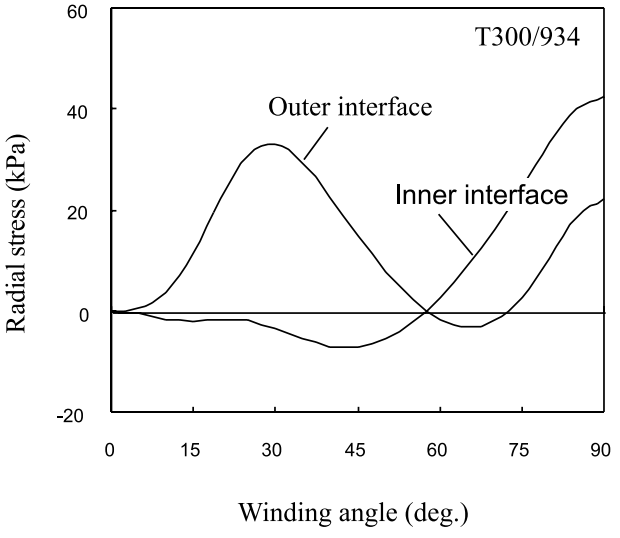

Fig. 8. Effect of the winding angle on the radial stresses of a pipe.

The stress and strain distributions of pipe wound at 55° are plotted in Figs. 9 and 10, respectively. The axial stresses have maximum stress distribution through the

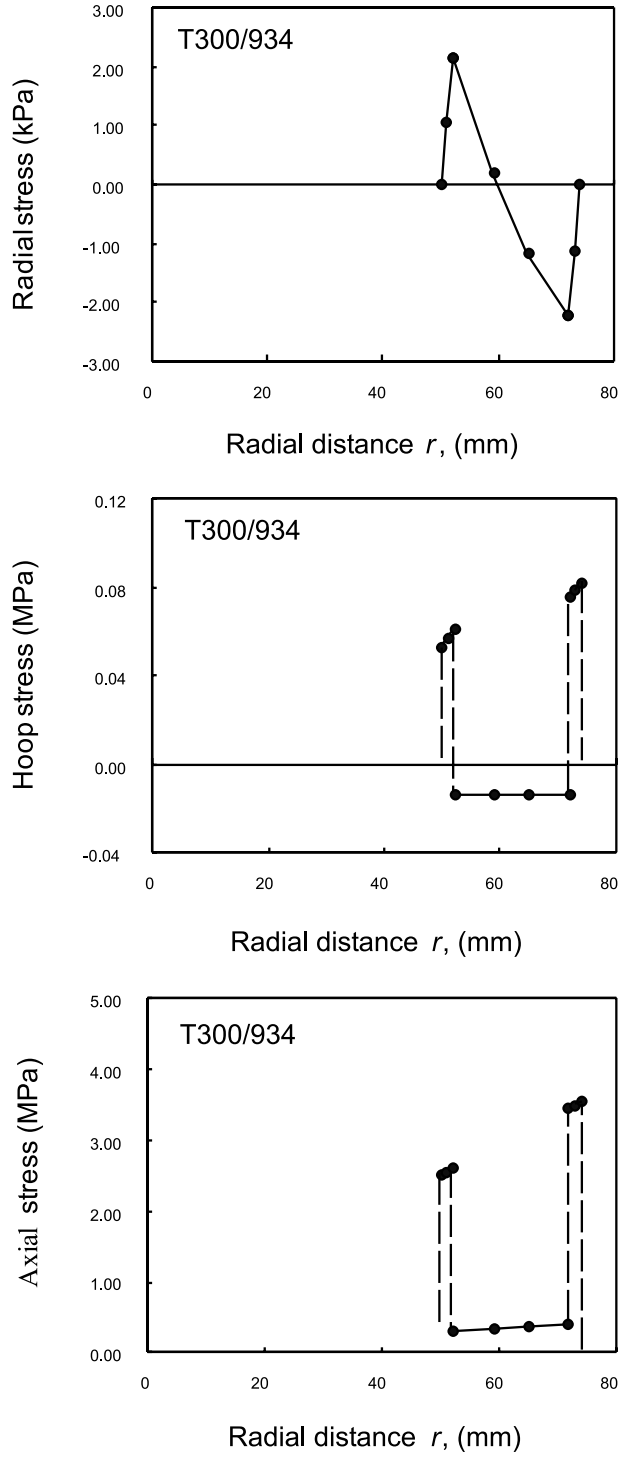

Fig. 9. Stress distribution within a sandwich pipe with a winding angle of 55°.

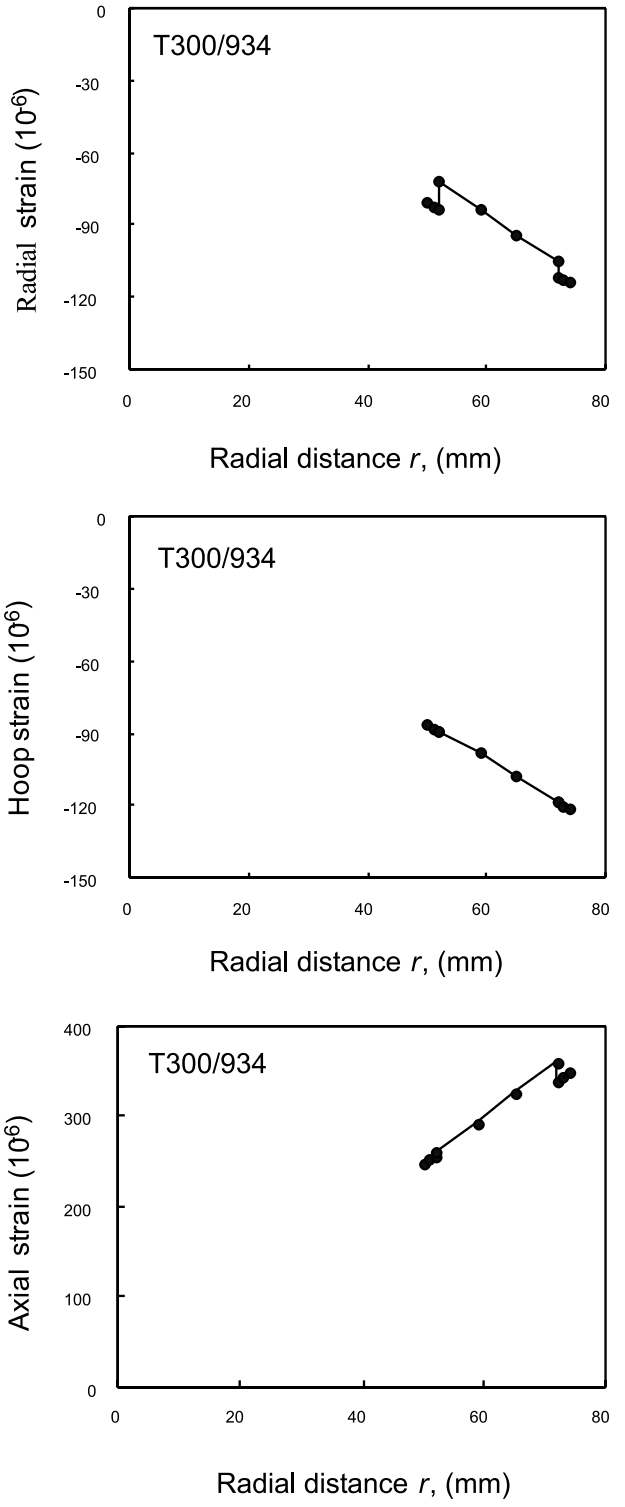

Fig. 10. Strain distribution within a sandwich pipe with a winding angle of 55°.

wall of the pipe. It is observed that the hoop and axial stresses have discontinuity at the interfaces but vary nearly linearly through the thickness direction of each layer. The radial stress displays a nonlinear distribution and is equal to zero at the inner and outer surfaces due to the free traction. For the hoop and axial stresses, the skin layers are subjected to much higher stresses than the core layer. As Fig. 10 shows, the three strains through the axial, hoop, and radial directions vary

discontinuously across the interfaces of the sandwich pipe. The axial strain remains tensile through the thickness direction, but compressive strains are observed in the radial and hoop directions.

Fig. 11 shows the axial and hoop strain curves at the inner and outer surfaces for pipes with different winding angles. It is observed that the inner surface can be subjected to larger strain than the outer surface in a pipe within certain winding angles, especially in a highly anisotropic composite pipe. The pipe is subjected to tensile axial strain because the inner and outer surfaces at $\theta = \pi/2$ are the tensile sides of the bending load.

Fig. 12 shows the deflection of the pipe at the outer surface through the cross-section of the sandwich pipe with a 55° winding angle. In Fig. 12, the cross-section after deformation is magnified a thousand times. It is observed that the radial displacement of the bottom surface is towards the center of the pipe. The axial compressive side (the bottom surface) of the pipe is subjected to buckling.

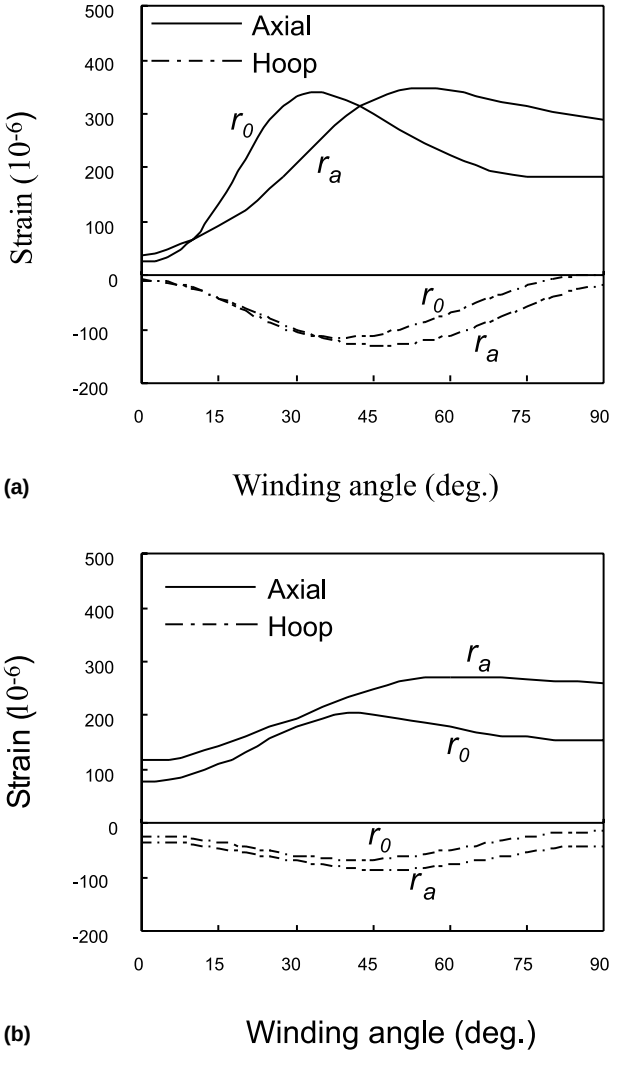

Fig. 11. Effect of the winding angle on the axial and hoop strains of pipe with (a) T300/934 and (b) E-glass/epoxy.

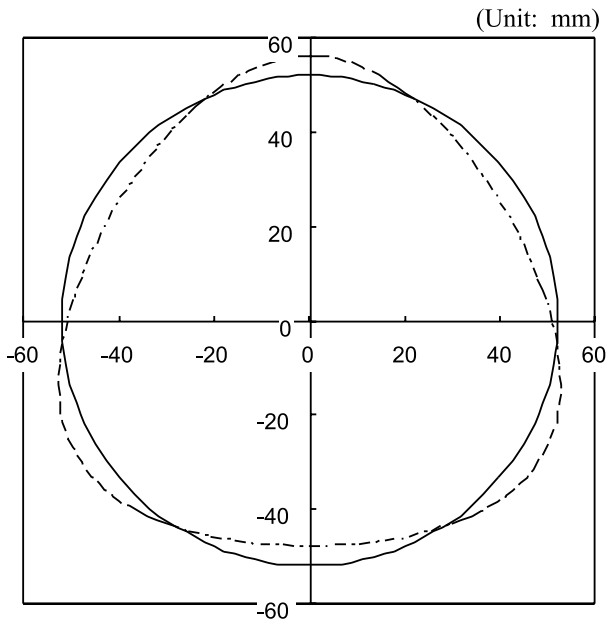

Fig. 12. Deformation at the outer surface through cross-section of pipe (1000×).

4. Conclusions

This research presents a method to analyze the stress–strain and deformation of a thick-walled filament-wound sandwich pipe under pure bending. The sandwich pipe is considered in 3D analysis and in an orthotropic-material model for the skin layers. The simple analytical method can be used to evaluate the stresses and deformation of multiple-layer cylindrical structures.

Detailed stresses and deformation of the filament-wound sandwich pipe subjected to bending load are investigated and discussed. It has been shown that the stresses and strains depend strongly on the winding angle when the pipe has the filament-wound layers with highly anisotropic composites such as T300/934. It is observed that the axial stresses and strains at the inner surface can be larger than those at the outer surface for a pipe within certain range of winding angles. The cross-section of a pipe is no longer a circle after the pipe is subjected to bending load.

Acknowledgements

Dr. M. Xia wishes to express his appreciation to the New Energy and Industrial Technology Development Organization (NEDO) for its financial support in the course of this study.

References

[1] Katayama T, Imadegawa K, Hirai T. Analysis of fracture mechanism of FW ring under impact load. In: Proceedings of the 71st JSME Fall Annual Meeting, 930-63A. 1993. p. 106–8 (in Japanese).

[2] Alderson KL, Evans KE. Failure mechanisms during the transverse loading of filament-wound pipes under static and low velocity impact conditions. Composites 1992;23:167–73.

[3] Hull D, Legg MJ, Spencer B. Failure of glass/polyester filament wound pipe. Composites 1978;9:17–24.

[4] Soden PD, Leadbetter D, Griggs PR, Eckold GC. The strength of a filament wound composite under biaxial loading. Composites 1978;9:247–50.

[5] Soden PD, Kitching R, Tse PC. Experimental failure stresses for ±55° filament wound glass fiber reinforced plastic tubes under biaxial loads. Composites 1989;20:125–35.

[6] Rosenow MWK. Wind angle effects in glass fiber-reinforced polyester filament wound pipes. Composites 1984;15:144–52.

[7] Spencer B, Hull D. Effect of winding angle on the failure of filament wound pipe. Composites 1978;9:263–71.

[8] Yamawaki K, Uemura M. Fracture strength of Helically wound composite cylinder: II Torsional strength. J Soc Mater Sci Jpn 1972;21:330–6 (in Japanese).

[9] Nishiwaki T, Yokoyama A, Maekawa Z, Hamada H, Mori S. A quasi-three-dimensional lateral compressive analysis method for a composite cylinder. Compos Struct 1995;32:293–8.

[10] Roy AK. Response of thick laminated composite rings to thermal stress. Compos Struct 1991;18:125–39.

[11] Yuan FG, Hsieh CC. Three-dimensional wave propagation in composite cylindrical shells. Compos Struct 1998;42:153–67.

[12] Cho H, Kardomateas GA, Valle CS. Elastodynamic solution for the shook stresses in an orthotropic thick cylindrical shell. ASME J Appl Mech 1998;65:184–93.

[13] Xia M, Kemmochi K, Takayanagi H. Analysis of multi-layered filament-wound composite pipes under internal pressure. Compos Struct 2001;53:483–91.

[14] Xia M, Takayanagi H, Kemmochi K. Analysis of filament-wound fiber reinforced sandwich pipe under combined internal pressure and thermomechanical loading. Compos Struct 2001;51:273–83.

[15] Xia M, Takayanagi H, Kemmochi K. Analysis of transverse loading for a laminated cylindrical pipe. Compos Struct 2001;53:279–85.

[16] Lo KH, Conway HD. Effect of change of Poisson's ratio on the bending of a multi-layered circular cylinder. Int J Mech Sci 1974;16:757–67.

[17] Lekhnitskii SG. Theory of elasticity of an anisotropic elastic body. San Franciso, CA: Holden-Day; 1963.

[18] Goetschel DB, Radford DW. Analytical development of through-thickness properties of composite laminates. J Adv Mater 1997;29(7):37–46.

[19] Greszczuk LB. Theoretical and experimental studies on properties and behavior of filamentary composites. In: Proceedings of the 21th Annual Meeting of SPI, Section 8-A, vol. 2. 1966.